Research Square

Preprints are preliminary reports that have not undergone peer review.
They should not be considered conclusive, used to inform clinical practice,
or referenced by the media as validated information.

Silicic acid-enhanced anodization coupled with one-step self- assembly toward universal superhydrophobic corrosion protection on magnesium alloys

Diqing Wan

divadwan@163.com

East China Jiaotong University

Mingyang He

East China Jiaotong University

Yi Xue

East China Jiaotong University

Short Report

Keywords: Magnesium alloy, Superhydrophobic coating, Anodization, Biomimetic hierarchical structure

Posted Date: November 25th, 2026

DOI: https://doi.org/10.21203/rs.3.rs-11531363/v1

License: This work is licensed under a Creative Commons Attribution 4.0 International License.
Read Full License

Additional Declarations: No competing interests reported.

Silicic acid-enhanced anodization coupled with one-step self-assembly toward universal superhydrophobic corrosion protection on magnesium alloys

Diqing Wan*, Mingyang He, Yi Xue

School of Materials Science and Engineering, East China Jiaotong University, Nanchang 330000, China;

*Correspondence: divadwan@163.com; Tel.: +86 13979175247

Abstract

Magnesium alloys have attracted extensive attention in aerospace, automotive and electronic fields due to their low density, high specific strength and high specific stiffness. However, their poor corrosion resistance has become a critical bottleneck restricting further application. Constructing superhydrophobic surfaces is an effective strategy to isolate corrosive media and impart multifunctional properties to magnesium alloys. Inspired by the superhydrophobic microstructure of lotus leaves, this work fabricated a biomimetic superhydrophobic coating on AZ31, AZ91 and ZK60 magnesium alloys via a facile anodization process combined with binary low-surface-energy substance self-assembly. Silicic acid-reinforced sodium silicate solution was used as the anodization electrolyte to construct a rough oxide layer with abundant reactive sites, and stearic acid (SA) and dodecyltrimethoxysilane (DTMS) were adopted for one-step co-modification. The effects of self-assembly time on surface morphology, wettability and corrosion resistance were systematically investigated. The results show that a typical micro-nano hierarchical structure mimicking lotus leaf surface is formed after 2 hours of self-assembly, with flower-like SA aggregates at micron scale and spherical DTMS aggregates at nanoscale. All modified magnesium alloys exhibit static water contact angles higher than 150°, presenting excellent water repellency and self-cleaning performance. Electrochemical tests indicate that the superhydrophobic coating significantly improves the corrosion resistance of magnesium alloys. The S-AZ91 sample possesses the optimal protective effect with a coating resistance of approximately 7135 $\Omega \cdot cm^2$, and its corrosion current density is reduced by approximately one order of magnitude compared with the bare substrate, which is comparable to many recently reported superhydrophobic coatings, though still inferior to some high-performance multilayer composite systems. This method has the advantages of simple operation, low raw material cost and wide substrate adaptability, showing great potential for industrial application of magnesium alloy surface protection.

Keywords: Magnesium alloy, Superhydrophobic coating, Anodization, Biomimetic hierarchical structure

1.Introduction

With the development of industry, the demand for lightweight materials and materials with special functions is growing increasingly higher[1-3]. Magnesium alloys possess advantages such as low density, high specific strength and high specific stiffness, which endow them with great applicability in aerospace, automotive parts, electronics and other fields[4-5]. However, the corrosion resistance of magnesium alloys has become a major bottleneck restricting their further development[6-7]. Magnesium alloys tend to react with water to form $Mg(OH)_2$, and this reaction proceeds continuously, which severely limits the application of magnesium alloys[8]. By constructing a superhydrophobic coating to isolate magnesium alloys from water contact, the application scope of magnesium alloys can be effectively expanded[9].

At present, the commonly used anti-corrosion technologies for magnesium alloys mainly include metallurgical methods and surface treatment methods[10]. Specifically, the surface treatment methods consist of chemical conversion coating, micro-arc oxidation technology, electroplating process, etc[11-12]. These methods prevent the corrosion of magnesium alloys based on different mechanisms, but compared with superhydrophobic coatings, they lack certain self-cleaning and anti-icing properties[13].

Superhydrophobicity provides an excellent approach for the corrosion protection of magnesium alloys, which achieves corrosion prevention while imparting additional functionalities [14]. In recent years, the fabrication of water-repellent surfaces by bionic imitation of lotus leaves, pitcher plants and other natural organisms has become a popular research topic[15-16]. Constructing a water-repellent surface on magnesium alloys can isolate the substrate from water contact, thereby completely inhibiting the occurrence of corrosion[17]. In addition, superhydrophobic surfaces also possess properties such as self-cleaning, anti-icing, anti-fouling and drag reduction[18]. Li[19-20] *et al*. developed an anodization method by adding silica sol to sodium silicate, and successfully prepared a superhydrophobic coating on AZ91D magnesium alloy. The results demonstrated that sodium silicate particles in this system are more likely to provide adsorbable ions, leading to a better film-forming effect. However, the preparation of silica sol is relatively cumbersome and costly. Zhou[21] *et al*. fabricated superhydrophobic surfaces using silica particles with different particle sizes, which constructed a bionic lotus leaf-like structure and exhibited excellent mechanical stability and durability, with a contact angle reaching 155 degrees. Nevertheless, the preparation of silica particles with two distinct particle sizes is rather challenging. Dai[22] *et al*. obtained a superhydrophobic surface with a contact angle of 154.60 degrees via in-situ growth of Mg-Al layered double hydroxides and modification with low surface energy materials, which reduced the corrosion current density by approximately five orders of magnitude.

In this study, inspired by the superhydrophobic microstructure of lotus leaf surfaces, a novel anodization method was developed to fabricate a rough surface, which was subsequently modified with two types of low surface energy substances to obtain a superhydrophobic surface.

The coating was prepared using silicic acid to form the sol; this method is simple and suitable for large-scale production. Meanwhile, by controlling the self-assembly time, the size of the superhydrophobic protrusions on the magnesium alloy surface was adjusted, thereby achieving a superior superhydrophobic effect. The resultant bionic coating exhibits excellent corrosion resistance and self-cleaning performance.

2.Experimental and Characterization

Hydrochloric acid is added to the sodium silicate solution to adjust the pH to slightly less than 7. The resulting silicic acid is washed, filtered, and fully dried at 40 °C to obtain the target silicic acid product. Then, 0.1 g of the prepared silicic acid and 1 g of sodium silicate were dissolved in 100 mL of deionized water to serve as the electrolyte. The duration of anodization is 5 minutes. Magnesium alloy samples (AZ31, AZ91, ZK60) with dimensions of 10 mm × 10 mm × 3 mm were ground successively with 400#, 800#, 1200# and 2000# SiC abrasive papers, ultrasonically cleaned in acetone and ethanol for 10 min each, and dried in air. A platinum sheet with an area of 1 cm^2 was used as the cathode, and the magnesium alloy is used as the anode. The applied voltage for anodization is set at 26 V. After the reaction is completed, the sample is fully dried at 90 °C. The specimens are immersed in an ethanol solution containing 5 vol% DTMS and 5 wt% SA, followed by thorough drying at 100 °C after removal. The treated specimens of AZ91 magnesium alloy are designated as S-AZ91, and the rest are named in the same manner.

Polarization curves and electrochemical impedance spectroscopy (EIS) tests are carried out using a Princeton 2273 electrochemical workstation. Surface morphology is characterized via a ZEISS Sigma 560 high-resolution thermal field-emission scanning electron microscope (FE-SEM), and elemental composition analysis is performed with its equipped energy dispersive spectrometer (EDS). The OCA15EC fully automatic contact angle measuring instrument is adopted to test the contact angle.

3.Results and discussion

To better illustrate the fabrication mechanism, a schematic diagram is proposed in Figure 1. The anodization process generates a porous oxide layer mainly composed of $Mg(OH)_2$ and $MgSiO_3$ on the magnesium alloy surface, providing abundant reactive hydroxyl groups. Upon immersion in the mixed ethanol solution, SA molecules preferentially react with $Mg(OH)_2$ via acid-base neutralization to form magnesium stearate, which self-assembles into micron-scale flower-like aggregates due to the strong hydrophobic interactions between long alkyl chains. Meanwhile, DTMS hydrolyzes and condenses with $MgSiO_3$ through siloxane bonds (Si-O-Si or Si-O-Mg), generating nano-scale spherical particles. The distinct polarity and different reactive sites of the two modifiers enable their independent nucleation and growth, ultimately forming a micro-nano binary hierarchical structure without mutual interference.

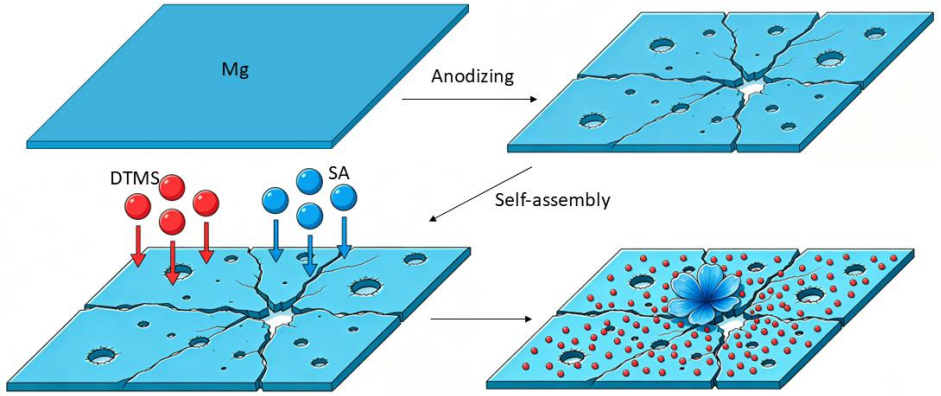


Figure 1. Schematic diagram of the coating fabrication process

Figure 2 displays SEM micrographs of the as-fabricated superhydrophobic surfaces. After 1 hour self-assembly (as shown in Figure 2a), ample low-surface-energy species precipitate on the alloy substrate, but no dual-scale micro/nanostructures are constructed. Extending the assembly duration to 2 h (as shown in Figure 2b) leads to the in-situ growth of flower-like large aggregates originating from SA, accompanied by tiny spherical DTMS-derived nanoparticles, as further verified in Figure 3. When the self-assembly time is prolonged to 4 hours, well-defined hierarchical architectures form, which are assembled by 3D network low-surface-energy films and densely packed spherical particle clusters.

The self-assembly duration of 1 hour is insufficient. Nano-spheres derived from DTMS form preferentially, while micron-sized flower-like structures of SA fail to develop completely, making it impossible to construct a micro-nano hierarchical rough structure. At 2 hours, SA generates micron-scale flower-like protrusions and DTMS produces nanoscale spherical particles. The two structures with complementary dimensions perfectly mimic the classic bionic structure of lotus leaf surfaces consisting of micron papillae and nano wax crystals. The binary hierarchical structure obtained after 2 hours of self-assembly can trap air to the greatest extent and drastically reduce the solid-liquid contact area, which serves as the structural foundation for the contact angle to exceed 150°. By contrast, continuous reticular layers composed of low-surface-energy substances form at 4 hours. These structures fill the micro-nano gaps and reduce air entrapment capacity, which theoretically leads to a slight deterioration in hydrophobicity. A single type of low-surface-energy material generally only constructs single-scale rough morphology[23]. In this work, SA and DTMS undergo independent nucleation and growth, spontaneously producing hierarchical structures with a broad dimensional range. This strategy achieves the desirable lotus leaf bionic effect more readily than modification with a single modifier.

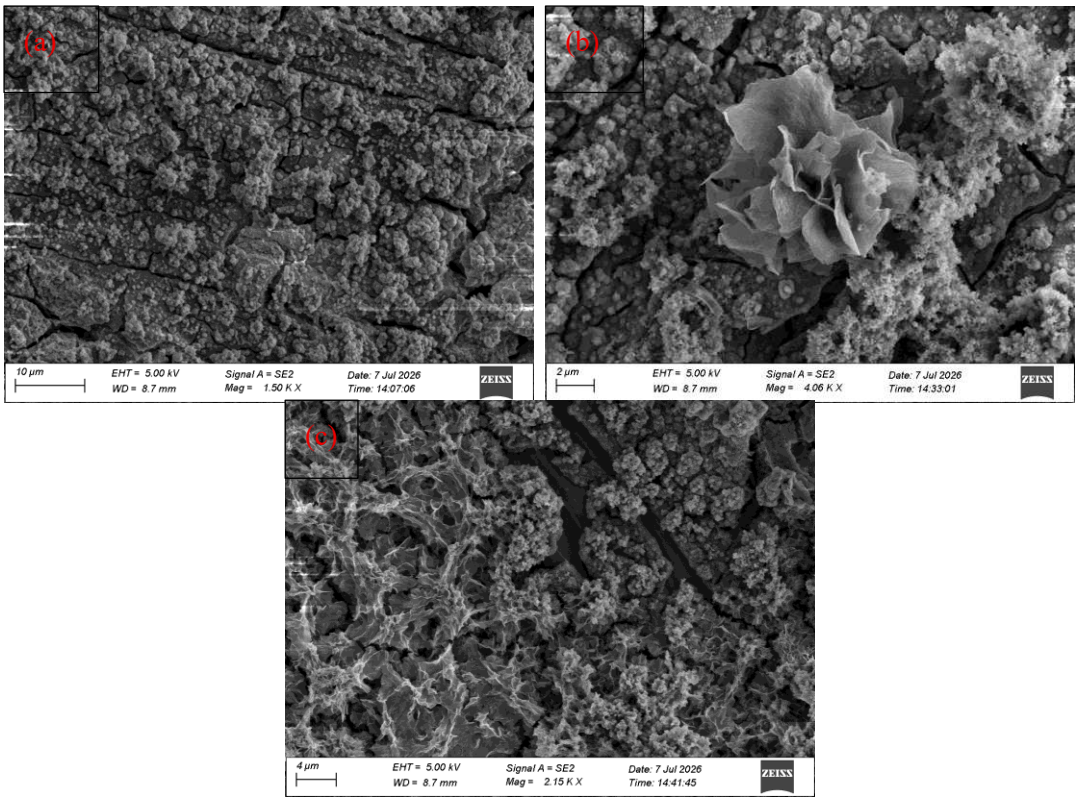


Figure 2. Microscopic morphologies of AZ31 magnesium alloy with different self-assembly durations [(a) 1 hour, (b) 2 hours, (c) 4 hours]

Figure 3 displays the EDS elemental mapping results of the magnesium alloy surface. The distribution of silicon element further verifies that DTMS is uniformly distributed on the alloy substrate. The discrepancy between carbon and silicon distributions sufficiently demonstrates that stearic acid (SA) and DTMS undergo separate self-assembly on the magnesium alloy surface. Meanwhile, the oxygen distribution confirms that abundant oxide compounds are extensively formed on the alloy after anodization. A large amount of $Mg(OH)_2$ and $MgSiO_3$ are produced on the magnesium alloy surface during anodization [19-20]. Subsequent reactions between these products with SA and DTMS respectively contribute to the fabrication of target low-surface-energy species.

$$Mg - 2e^- = Mg^{2+} \quad (1)$$

$$Mg(OH)_2 + SA = Mg(OH)_2 - SA \quad (2)$$

$$MgSiO_3 + DTMS = DTMS - MgSiO_3 \quad (3)$$

The separate self-assembly behavior of SA and DTMS originates from their fundamentally different molecular structures and reaction chemistries. SA, as a long-chain fatty acid, possesses a polar carboxyl head (-COOH) and a nonpolar alkyl tail ($-C_{17}H_{35}$). Its grafting to the substrate relies on the deprotonation of -COOH and subsequent coordination with Mg^{2+} from $Mg(OH)_2$, forming magnesium stearate with an ionic bond character(Equation 2). The strong van der Waals interactions among the alkyl chains drive the lateral aggregation of SA molecules, leading to the formation of micron-sized flower-like structures.

In contrast, DTMS is a silane coupling agent with three hydrolyzable methoxy groups (-OCH_3). In the ethanol solution with trace water, DTMS undergoes hydrolysis to form silanol groups (-SiOH), which then condense with the -OH groups on $MgSiO_3$ surface to form covalent Si-O-Si or Si-O-Mg bonds (as shown in Equation 3). The sol-gel nature of silane chemistry favors the formation of spherical nanoparticles via homogeneous nucleation. Furthermore, the limited concentration of each modifier in the mixed solution (5wt% and 5vol%) ensures that the nucleation and growth of SA and DTMS occur independently without forming mixed aggregates, as verified by the elemental mapping results (as shown in Figure 3).

After anodization, the magnesium alloy surface not only gains increased roughness. During anodization, the substrate reacts with silicic acid and water to generate abundant hydroxyl-rich active sites on the surface. On the one hand, $Mg(OH)_2$ undergoes an acid-base reaction with SA; on the other hand, $MgSiO_3$ reacts with DTMS via siloxane grafting. The low-surface-energy substances are immobilized on the alloy surface through chemical bonds, which endows the coating with much higher stability compared with physical adsorption. The inconsistent distribution of carbon-rich and silicon-rich regions verifies that SA and DTMS anchor at distinct assembly sites rather than undergoing simple co-deposition. The uniform dispersion of silicon element confirms the homogeneous modification by DTMS across the entire surface, guaranteeing surface uniformity. According to previous literature, single-component modification systems using only SA or DTMS have been widely reported[24-25]. In this work, simultaneous grafting of the two components is realized within a single mixed solution system. A micro-nano dual-scale hierarchical structure is successfully constructed via identical reaction pathways. This simplified preparation route delivers superior superhydrophobic performance compared with conventional single-component modification strategies.

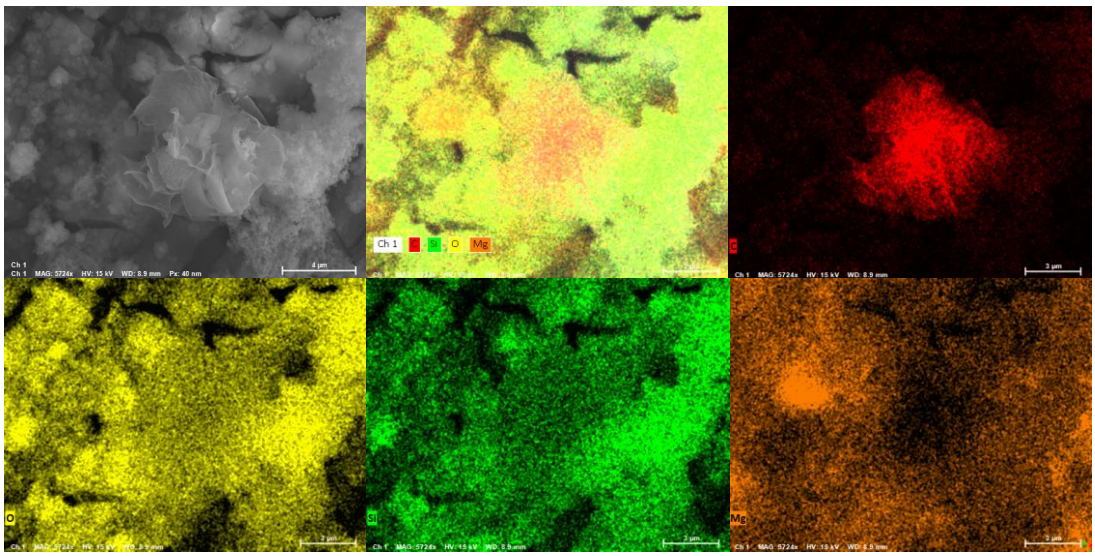


Figure 3. EDS elemental mapping of AZ31 Mg alloy subjected to 2 h self-assembly

Figure 4 presents the static contact angles of three kinds of magnesium alloy substrates after superhydrophobic modification, all of which exceed 150°. The flushing test under continuous

water flow is displayed in the following figure. It can be observed that water flows onto the alloy surface from the top and bounces off directly, indicating that the alloy surface achieves favorable hydrophobic performance.

Three commercial magnesium alloys with distinctly different compositions, namely AZ31, AZ91 and ZK60, all achieve superhydrophobicity after identical treatment procedures, demonstrating that this fabrication method is not limited to specific alloying elements. The underlying mechanism lies in the fact that anodization can produce hydroxyl-containing magnesium oxide layers on any magnesium alloy substrate, which provide universal reactive active sites. Accordingly, this process possesses great potential for engineering application and large-scale promotion. Water droplets bounce off the surface immediately with negligible residual liquid, qualitatively suggesting that the surface likely follows the Cassie-Baxter wetting regime rather than the Wenzel state. The trapped air layer within the hierarchical structure produces an air cushion effect, which provides the fundamental basis for self-cleaning ability. The water flushing test qualitatively demonstrates that the surface exhibits good water repellency; however, quantitative dynamic contact angle and rolling angle measurements are still needed in future work to fully evaluate the dynamic wetting behavior.

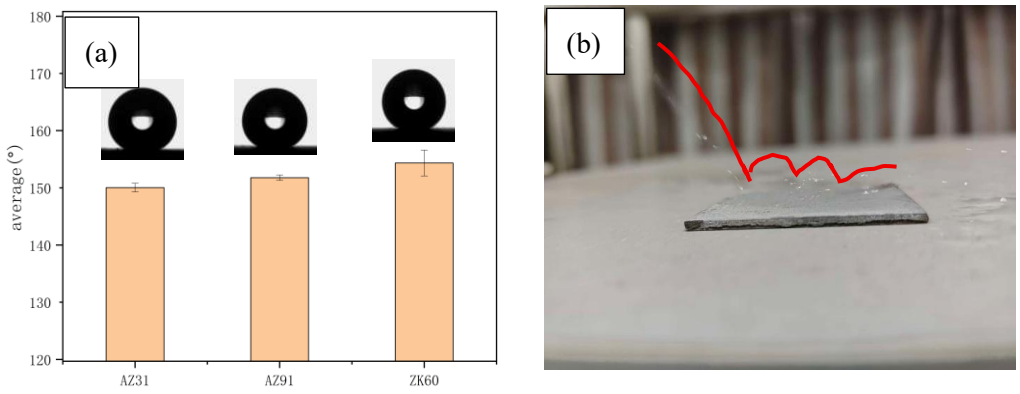


Figure 4. Static water contact angles and water flushing test for three Mg alloys (Left: contact angle photographs; Right: water flushing demonstration)

The water flushing test (Fig4b) qualitatively reveals that water droplets readily detach from the surface under flowing water, implying a low adhesion force. However, a more rigorous evaluation of dynamic hydrophobicity, including sliding angle measurement and droplet impact tests, will be performed in our future work to fully characterize the self-cleaning performance. The corrosion current density of the treated alloy is reduced by approximately one order of magnitude compared with the untreated counterpart. Considering that the corrosion current density is highly dependent on testing conditions, a direct quantitative comparison should be made with caution. Nevertheless, within the same electrolyte (3.5 wt% NaCl), the corrosion current density of our coated samples(Fig.5) falls within the same order of magnitude as most of the previously reported values listed in Table 1, indicating that the present coating provides a level of protection comparable to many existing superhydrophobic coatings on magnesium alloys[27-32], the corrosion current density obtained in this work falls within the same order of

magnitude.

Table 1. Comparison of Current Densities of Alloys

Author	I_corr (μA·cm⁻²)	Alloy	Electrolyte
Qi	0.91224	AZ91	3.5 wt% NaCl
Cao	3.96	AZ91	3.5 wt% NaCl
Wan*	**4.63**	**AZ91**	**3.5 wt% NaCl**
Wu	0.871	AZ31	3.5 wt% NaCl
Zhang	0.30	AZ31	3.5 wt% NaCl
Wan*	**9.64**	**AZ31**	**3.5 wt% NaCl**
Wang	1.52	ZK60	3.5 wt% NaCl
Qiu	14.39	ZK60	3.5 wt% NaCl
Wan*	**5.50**	**AZ91**	**3.5 wt% NaCl**

Note: The corrosion current densities from different references were measured under various test conditions (e.g., scan rate, potential range), which may affect the absolute values. The data are provided for qualitative comparison only. The values marked with * denote the results from the same research group for direct comparison.

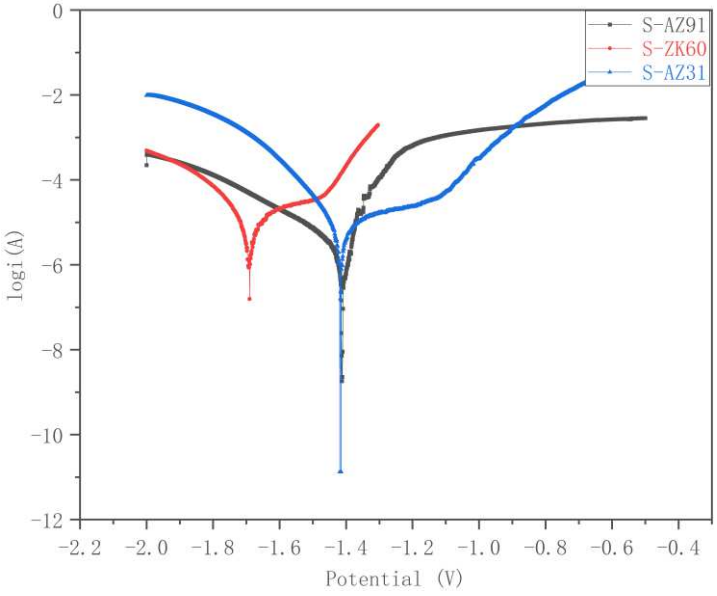


Figure 5. Potentiodynamic polarization curves of three magnesium alloys

Figure 6 shows the electrochemical impedance spectra of the alloys subjected to 2 hours self-assembly treatment. The fitting parameters of the corresponding equivalent circuit are listed in Table 2. The Nyquist plots of all three samples exhibit a single capacitive semicircle, indicating that the electrochemical response is dominated by the barrier property of the superhydrophobic coating. Therefore, a single-time-constant equivalent circuit Rs(CPE1-R1) was employed for fitting, where R1 represents the total resistance of the coating layer. The fitting results are listed in Table 2. Among the three groups of specimens, S-AZ91 possesses the maximum impedance value of approximately 7000 Ω·cm². Even with identical modification procedures, different substrate alloys exhibit distinct corrosion resistance.

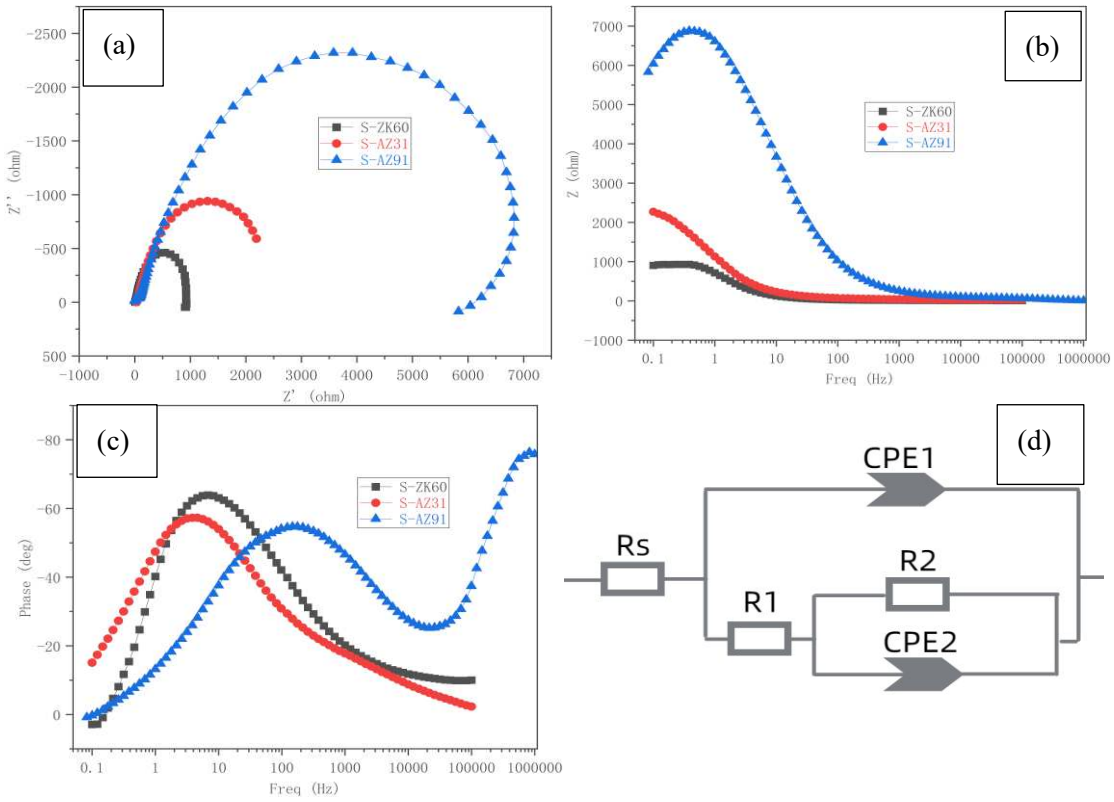


Figure 6. Electrochemical impedance spectra of the three alloys after 2 h self-assembly treatment: (a) Nyquist plots, (b/c) Bode impedance modulus and phase angle plots, (d) The inset shows the equivalent circuit used for fitting

Table 2. Fitted EIS parameters of the three alloys

Sample	Rs	R1	CPE1		R2	CPE2	
	($\Omega \cdot cm^2$)	($\Omega \cdot cm^2$)	$Y_0(\Omega^{-1}cm^2s^n)$	n	($\Omega \cdot cm2$)	$Y_0(\Omega^{-1}cm^2s^n)$	n
S-ZK60	10.36	1113	2.68×10^{-4}	0.78	_	_	_
S-AZ31	31.79	3362	2.40×10^{-4}	0.68	_	_	_
S-AZ91	0.96	7135	1.01×10^{-5}	0.70	79.23	1.50×10^{-8}	0.99

Overall, the corrosion current densities of AZ31, AZ91 and ZK60 alloys after the anodization and binary self-assembly treatment are located in the same order of magnitude as those of most

recently reported magnesium alloy superhydrophobic coatings[27-32]. This result demonstrates that the fabrication strategy proposed in this work can deliver reliable corrosion protection for magnesium alloys, and the protective performance reaches the mainstream level of this research field, verifying the feasibility of this method.

From the perspective of preparation technology, although some approaches including femtosecond laser ablation, in-situ growth of layered double hydroxide (LDH) have achieved comparable or even superior corrosion resistance, these methods generally have inherent drawbacks that hinder large-scale industrial application. For instance, femtosecond laser processing requires high-precision and expensive equipment, which suffers from low processing efficiency for large-area components and poor adaptability to workpieces with complex curved surfaces. The hierarchical structure constructed by dual-size silica particles involves pre-synthesis of monodisperse nanoparticles with targeted sizes, leading to complicated procedures and poor process controllability. As for the conventional anodization system with silica sol additive, the cumbersome preparation of silica sol precursor also increases the process complexity and production cost. In comparison, the superhydrophobic coating in this study is constructed by a silicic acid-reinforced sodium silicate anodization process, followed by one-step co-self-assembly modification with SA and DTMS. The whole fabrication route is free of precision instruments and complex precursor synthesis. With low-cost and easily available raw materials as well as simple and controllable operation, this method is compatible with magnesium alloy workpieces of various sizes and geometries, exhibiting remarkable advantages in scalable manufacturing over most existing strategies.

Nevertheless, it should be acknowledged that the corrosion current density of the coated sample is only reduced by about one order of magnitude compared with the bare substrate. Compared with some high-performance multilayer composite superhydrophobic coatings (e.g., the biomimetic LDH coating with corrosion current reduced by five orders of magnitude[22]), the barrier protection capability of the current coating still has considerable room for improvement. This performance gap is mainly ascribed to the limited thickness and compactness of the anodic oxide film obtained under the present process parameters, which allows corrosive media to penetrate gradually through the intrinsic defects of the film. Future work can further enhance the physical shielding effect of the anodic base layer by optimizing anodization parameters, introducing nanoparticle doping, or loading corrosion inhibitors, to achieve a better balance between protective performance and process simplicity.

Conclusion

In this work, a biomimetic lotus-leaf superhydrophobic coating was fabricated on AZ31, AZ91 and ZK60 magnesium alloys via a silicic acid-enhanced anodization process combined with one-step co-self-assembly of SA and DTMS. The surface microstructure, elemental distribution, wettability and corrosion resistance of the coatings were systematically characterized.

(1) The results demonstrate that self-assembly time plays a key role in regulating the surface

hierarchical structure. After 2 h of assembly, micron-sized flower-like SA aggregates and nano-sized spherical DTMS particles coexist on the surface, forming a typical micro-nano binary structure that highly replicates the topography of natural lotus leaves. All three modified magnesium alloys achieve static water contact angles above 150°, presenting favorable water repellency and self-cleaning performance.

(2) Electrochemical tests verify that the superhydrophobic coating significantly enhances the corrosion resistance of magnesium alloys through the synergistic effect of the composite oxide layer's physical barrier and the trapped air layer's insulation. The S-AZ91 sample exhibits the optimal protective effect with a coating resistance of 7135 $\Omega \cdot cm^2$, and its corrosion current density is reduced by approximately one order of magnitude compared with the bare substrate, which is comparable to the performance level of many reported superhydrophobic magnesium alloy coatings. Nevertheless, the corrosion current density reduction (about one order of magnitude) remains lower than that of some advanced multilayer composite coatings (up to 3-5 orders of magnitude), indicating considerable room for further improvement through optimizing the compactness of the anodic base layer.

(3) Compared with conventional preparation strategies, this method has the advantages of simple operation, low-cost raw materials and wide substrate adaptability, showing great potential for large-scale industrial application. Future work will further optimize the compactness of the anodic base layer and the mechanical stability of the coating to improve its long-term service performance.

Reference

[1] Simões S. High-performance advanced composites in multifunctional material design: State of the art, challenges, and future directions[J]. Materials, 2024, 17(23): 5997.

[2] Patel V, Sharma P, Tiwari A, et al. Magnesium alloys in the automotive industry: Alloying elements and their impact on material performance[J]. Global Journal of Engineering and Technology Advances, 2024, 21(01): 130-145.

[3] Chen X, Yuan Y, Zhou X, et al. Harnessing the power of α-Mg: Unveiling the matrix phase's role in Mg alloys from structure to function[J]. Journal of Magnesium and Alloys, 2025.

[4] Zhu Z, Ayoub I, He J, et al. Magnesium alloys with rare-earth elements: Research trends applications, and future prospect[J]. Journal of Magnesium and Alloys, 2025.

[5] Xin T, Zhao Y, Mahjoub R, et al. Ultrahigh specific strength in a magnesium alloy strengthened by spinodal decomposition[J]. Science Advances, 2021, 7(23): eabf3039.

[6] Gao X, Zhu Z, Zhang H D, et al. Research progress on corrosion behavior of magnesium alloy composites in practical service conditions[J]. Advanced Sustainable Systems, 2025, 9(10): e00660.

[7] Singh G, Singh S, Sidhu S S. Corrosion protection of magnesium alloys by electrophoretic deposition: recent developments and future perspectives[J]. Surface Engineering, 2026, 42(2): 137-165.

[8] Persson D, Wärnheim A, LeBozec N, et al. Studies of Initial Atmospheric Corrosion of Magnesium Alloys AZ91 and AZ31 with Infrared Spectroscopy Techniques[J]. Corrosion and Materials Degradation, 2025, 6(4): 59.

[9] Yu X, Zhang M. Sprayable Graphene Oxide-Based Superhydrophobic Coating with High Mechanical/Chemical Stability and Self-Healing Performance for Corrosion Protection of Mg Alloys[J]. Langmuir, 2025, 41(31): 20824-20835.

[10] Wu T, Zhang K. Corrosion and protection of magnesium alloys: recent advances and future perspectives[J]. Coatings, 2023, 13(9): 1533.

[11] Tan J, Liu L, Wang H, et al. Advances in anti-corrosion coatings on magnesium alloys and their preparation methods[J]. Journal of Coatings Technology and Research, 2024, 21(3): 811-825.

[12] Gao X, Zhu Z, Zhang H D, et al. Research progress on corrosion behavior of magnesium alloy composites in practical service conditions[J]. Advanced Sustainable Systems, 2025, 9(10): e00660.

[13] Wang Y, Feng L. Fabrication and Multifunctional Performance of Ce-Based Superhydrophobic Coating on AZ91D Magnesium Alloy[J]. AIP Advances, 2025, 15(8): 085319.

[14] Cai Q, Xu J, Xu A, et al. Magnesium Alloy Composite Water-Repellent Surface with Durable Corrosion Resistance and Self-Cleaning Behavior[J]. Advanced Engineering

Materials, 2024, 26(7): 2301936.
[15] Alias H, Alias J, Alang N A. Anticorrosion strategy for magnesium alloys through a superhydrophobic approach utilizing slippery liquid-infused porous surface coating[J]. Journal of Coatings Technology and Research, 2025, 22(2): 491-510.
[16] Guittard F, Amigoni S, Darmanin T. Bioinspired and Biomimetic Wetting Properties[J]. ACS nano, 2025, 19(41): 36005-36026.
[17] Zhang Y, Li N, Ling N, et al. Enhanced long-term corrosion resistance of Mg alloys by superhydrophobic and self-healing composite coating[J]. Chemical Engineering Journal, 2022, 449: 137778.
[18] Zhang Y, Fan X, Li X, et al. Micro-structure design of black ceramic composite surface towards photothermal superhydrophobic anti-icing[J]. Chemical Engineering Journal, 2024, 498: 155101.
[19] Li W, Zhu L, Liu H. Preparation of hydrophobic anodic film on AZ91D magnesium alloy in silicate solution containing silica sol[J]. Surface and Coatings Technology, 2006, 201(6): 2573-2577.
[20] Zhu L, Li Y, Li W. Influence of silica sol particle behavior on the magnesium anodizing process with different anions addition[J]. Surface and Coatings Technology,2008,202(24):5853-5857.
[21] Zhou N, Hou S, Noh I, et al. Constructing robust and multifunctional superamphiphobic surfaces by using two different nanostructures of silicon dioxide[J]. Langmuir, 2025, 41(9): 6376-6388.
[22] Dai L, Cui H, Chen X, et al. A multi-level biomimetic LDH coatings with super hydrophobicity, corrosion resistance, anti-icing and anti-fouling properties on magnesium alloy[J]. Journal of Magnesium and Alloys, 2025.
[23] Wang L, Zhang J L. Enhanced long-term corrosion resistance of Mg alloys by superhydrophobic and self-healing composite coating[J]. Chemical Engineering Journal, 2022, 445: 136672.
[24] Zhang S, Li M, Li B, et al. Corrosion resistance of a superhydrophobic polypropylene coating on magnesium alloy AZ31[J]. Anti-Corrosion Methods and Materials, 2024, 71(5): 543-554.
[25] Cui X, Lin X, Liu C, et al. Fabrication and corrosion resistance of a hydrophobic micro-arc oxidation coating on AZ31 Mg alloy[J]. Corrosion Science, 2015, 90: 402-412.
[26] Bi P, Li H, Zhao G, et al. Robust super-hydrophobic coating prepared by electrochemical surface engineering for corrosion protection[J]. Coatings, 2019, 9(7): 452.
[27] Qi, S; Liu, X; Cheng, L; Zhu, J. Superhydrophobic Corrosion-Resistant Coating of AZ91D Magnesium Alloy: Preparation and Performance. *Coatings* **2024**, *14*, 1237.
[28] Cao J, Ma B, Li L, et al. Research on the mechanism of femtosecond laser ablation concave-convex microstructure transformation[J]. Langmuir, 2024, 40(44): 23218-

23229.

[29] Wu, Z, Liu, Y, Zhang, Y. *et al.* The effect of micro/nanostructures formed by laser ablation on the superhydrophobicity of AZ31B magnesium alloy. *Journal of Materials Research* **39**, 850–863 (2024).

[30] Zhang, H, Cai, S, Zhang, H. *et al.* Corrosion behavior and antibacterial adhesion of superhydrophobic composite coatings on AZ31 magnesium alloys. *J Coat Technol Res* **21**, 1663–1675 (2024).

[31] Wang, Y, Ba, Z, Xu, D. *et al.* Ultrasonic-Assisted Fabrication of Superhydrophobic Mg-Mn Layered Double Hydroxides Coating on ZK60 Magnesium Alloy and Its Properties. *J. of Materi Eng and Perform* **31**, 7596–7608 (2022).

[32] Qiu Z, Sun J, Wang R, et al. Magnet-induced fabrication of a superhydrophobic surface on ZK60 magnesium alloy[J]. Surface and Coatings Technology, 2016, 286: 246-250.

Funding: This work was supported by the National Natural Science Foundation of China [grant number 52561027].

Competing interests: The authors declare that they have no competing interests.

Availability of data and materials: The datasets generated and/or analysed during the current study are available from the corresponding author on reasonable request.